Acta Crystallographica Section F
Structural Biology and Crystallization Communications
ISSN 1744-3091

Dramatic improvement of crystal quality for low-temperature-grown rabbit muscle aldolase

HaJeung Park,[a] Erumbi S. Rangarajan,[a] Jurgen Sygusch[b]* and Tina Izard[a]

[a]Cell Adhesion Laboratory, Department of Cancer Biology, The Scripps Research Institute, Jupiter, FL 33458, USA, and [b]Département de Biochimie, Université de Montréal, Montréal, Québec H3C 3J7, Canada

Correspondence e-mail: jurgen.sygusch@umontreal.ca

Received 24 November 2009
Accepted 29 March 2010

Rabbit muscle aldolase (RMA) was crystallized in complex with the low-complexity domain (LC4) of sorting nexin 9. Monoclinic crystals were obtained at room temperature that displayed large mosaicity and poor X-ray diffraction. However, orthorhombic RMA–LC4 crystals grown at 277 K under similar conditions exhibited low mosaicity, allowing data collection to 2.2 Å Bragg spacing and structure determination. It was concluded that the improvement of crystal quality as indicated by the higher resolution of the new RMA–LC4 complex crystals was a consequence of the introduction of new lattice contacts at lower temperature. The lattice contacts corresponded to an increased number of interactions between high-entropy side chains that mitigate the lattice strain incurred upon cryocooling and accompanying mosaic spread increases. The thermodynamically unfavorable immobilization of high-entropy side chains used in lattice formation was compensated by an entropic increase in the bulk-solvent content owing to the greater solvent content of the crystal lattice.

1. Introduction

The quality of X-ray diffraction data from protein crystals is dictated by the physical properties of the crystals, which influence their maximum resolution of observed X-ray diffraction, signal-to-noise ratio, redundancy and mosaicity, and by the diffraction apparatus, such as the quality of the X-ray source and the tuning of the detector and goniostat. The tremendous advances in diffraction instrumentation leave little room for improving the quality of the diffraction data by modification of the diffraction apparatus. Thus, the focus has been directed towards improvement of crystal quality. Many methods have been elaborated for improvement of the quality of X-ray diffraction data and these include optimization of the crystallization conditions and manipulation of crystals after they are fully grown. Such attempts include, but are not limited to, reduction of the nucleation rate, microseeding and macroseeding, microgravity crystallization, protein surface mutation, cryocrystal annealing, change in humidity of the crystal and cross-linking (Bergfors, 1999; Ng *et al.*, 1997; Yeh & Hol, 1998; Kiefersauer *et al.*, 2000; Derewenda & Vekilov, 2006; Izard *et al.*, 1997; Hurlbert & Izard, 2002; Ellis *et al.*, 1999). Of these methods, diminishing the rate of nucleation is perhaps the most commonly used as a first attempt to achieve improvement of crystal quality and can be accomplished by manipulating the protein concentration, precipitant concentration and temperature.

Crystals of the unliganded form of rabbit muscle aldolase (RMA) were first reported by Eagles *et al.* (1969) and the first structure was described by Sygusch *et al.* (1987). Since then, numerous crystal structures with various ligands have been reported. A total of 16 RMA crystal structures have been deposited in the Protein Data Bank to date and include both unliganded RMA as well as RMA in complex with small molecules. With the exception of two crystal forms, namely PDB entries 2ot0 (RMA in complex with a peptide ligand; St-Jean *et al.*, 2007) and 1fdj (RMA in complex with an enzymatic intermediate; N. S. Blom, A. White & J. Sygusch, unpublished work), all of the other 14 structures reported were crystallized in one of two crystal forms: form *A*, which has approximate unit-cell parameters $a = 164$, $b = 58$, $c = 85$ Å, $\beta = 102.7^\circ$ and is represented by PDB entry 1ado (Blom & Sygusch, 1997), and form *B*, which has

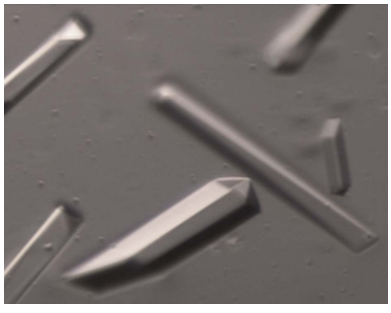

© 2010 International Union of Crystallography
All rights reserved

approximate unit-cell parameters $a = 85$, $b = 104$, $c = 84$ Å, $\beta = 98.7^\circ$ and is represented by PDB entry 2ot1 (St-Jean *et al.*, 2007). Both crystals forms (*A* and *B*) were grown at room temperature and crystallized in space group $P2_1$, but with different unit-cell parameters (see above). Independent of their crystal forms, X-ray diffraction data of all RMA crystals in complex with a ligand resulted in a mosaic spread of between 0.5° and 1.2°.

More recently, we have crystallized and solved a new liganded form of RMA in complex with the low-complexity domain (LC4) of sorting nexin 9 (Rangarajan *et al.*, 2010). As for all other RMA crystals, the crystallization conditions were initially screened and optimized at room temperature, but poor crystal quality prevented the collection of a full X-ray diffraction data set. However, growing these RMA–LC4 crystals at lower temperature with lower protein and reservoir concentrations dramatically improved the diffraction limit compared with such crystals grown at room temperature, and allowed X-ray diffraction data collection and structure determination. Moreover, we have observed a dramatic improvement in the mosaic spread for these crystals compared with all other liganded RMA crystals. Here, we report the improvement of RMA–LC4 crystal quality by lowering the crystallization temperature and the concentration of the protein and precipitant. By comparing the crystal packing of our RMA–LC4 crystals with those of other RMA–ligand crystals, we interpret the reduced mosaic spread as a consequence of increased interactions between high-entropy side chains whose thermodynamically unfavorable immobilization is compensated for by an entropic increase in bulk solvent, owing to the crystal lattice packing.

2. Materials and methods

2.1. Crystallization

We initially screened our RMA–LC4 complex for optimal crystallization conditions using the sparse-matrix method at room temperature with 15 mg ml^{-1} protein and a 1:3 molar excess of LC4 peptide. The final crystallization condition from the room-temperature screening was 25% PEG MME 550, 100 m*M* Tris–HCl pH 7.1 and 10 m*M* $MgCl_2$. Reproducing this condition in large hanging drops resulted in numerous small crystals that appeared within 24 h, indicating very strong nucleation, and only occasionally produced single crystals with sharp edges. In an attempt to reduce the nucleation rate, crystallization was repeated after reducing both the protein and the precipitant concentrations, which resulted in long needle-shaped crystals that appeared at 277 K; no crystals appeared at room temperature. The optimized crystallization condition at 277 K was 14% PEG MME 550, 100 m*M* Tris–HCl pH 7.6 and 10 m*M* $MgCl_2$, while the protein concentration was 10 mg ml^{-1} (Fig. 1).

2.2. Data collection and structure determination

We cryocooled our RMA–LC4 crystals grown at either temperature by including 20% ethylene glycol in the well solution. We collected data to 2.2 Å Bragg spacing on a MAR 225 CCD detector at the Southeast Regional Collaborative Access Team (SER-CAT) 22-BM beamline at the Advanced Photon Source, Argonne National Laboratory (Fig. 2). The data set was processed with *HKL*-2000 (Otwinowski & Minor, 1997). The RMA–LC4 complex crystallized in space group $P2_12_12_1$, with unit-cell parameters $a = 87.03$, $b = 118.18$, $c = 175.9$ Å. Crystals grown at room temperature displayed similar unit-cell parameters and mosaicity (of about 1°) as found for PDB entry 2ot0. Rigid-body refinement using PDB entry 2ot0 and the program *PHENIX* v.1.5 (Adams *et al.*, 2002) confirmed that the room-temperature-grown crystals indeed have the same crystal packing as found for the RMA–WASP crystals (data not shown).

Structure determination of the crystals grown at 277 K was performed by molecular replacement using the program *MOLREP* (Vagin & Teplyakov, 1997); a monomer of RMA from PDB entry 1ado was used as the search model. Refinement was performed with *PHENIX* v.1.5 (Adams *et al.*, 2002) and *autoBUSTER* (Blanc *et al.*, 2004) with iterative cycles of manual inspection of structures using *Coot* (Emsley & Cowtan, 2004). For comparison, we reprocessed the X-ray diffraction data to 2.2 Å Bragg spacing from our previously published 2.05 Å structure of the RMA–WASP (PDB entry 2ot0) and RMA–NASEP (PDB entry 2ot1) complexes and subsequently refined the structures by performing a macrocycle of *autoBUSTER* with noncrystallographic symmetry restraints. Details of the data-reduction and crystallographic refinement statistics can be found in Tables 1 and 2, respectively. Structure analysis was performed with the molecular-modeling graphics programs *Coot* and *PyMOL* (DeLano, 2002). A Ramachandran plot analysis using the program *PROCHECK* (Collaborative Computational Project, Number 4, 1994) indicates that 93.6, 91.8 and 92.5% of all residues lie in most favorable regions and 6.4, 8.2 and 7.5% are in additional allowed regions for the RMA–LC4, RMA–WASP and RMA–NASEP complexes, respectively, and that all stereochemical parameters are better than expected at the given resolution. Generation and inspection of crystal packing were aided by *PISA* (Krissinel & Henrick, 2007). Detailed structural descriptions of RMA–WASP and RMA–NASEP have been published (St-Jean *et al.*, 2007).

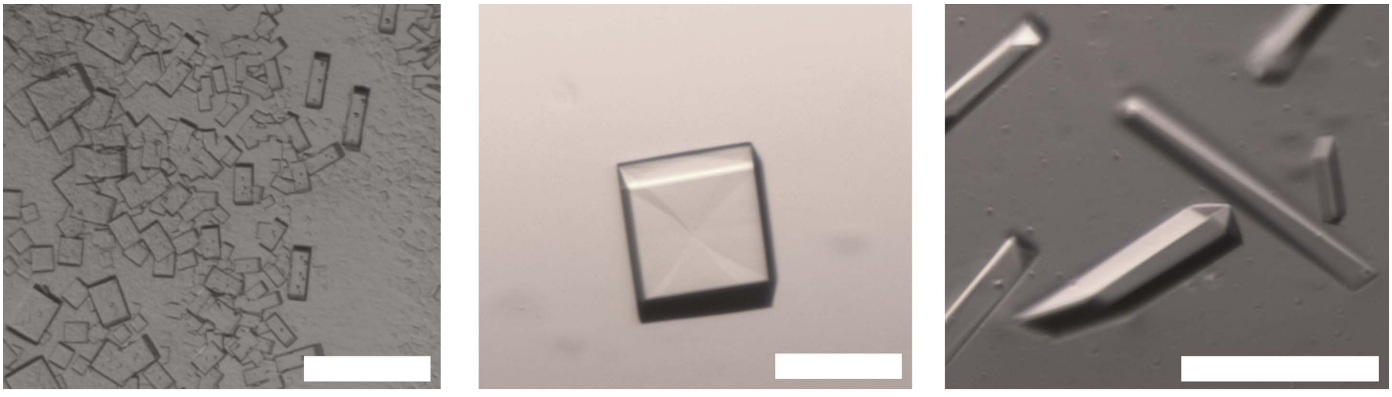

(*a*) (*b*) (*c*)

Figure 1
Comparison of crystal morphologies of RMA–LC4. (*a*) Initial crystallization showers obtained at room temperature; (*b*) optimized monoclinic room-temperature crystals; (*c*) orthorhombic crystals obtained at 277 K. The solid bar corresponds to 0.1 mm.

Table 1
Data-reduction statistics for three aldolase complex data sets.

Values in parentheses are for the highest resolution shell

	RMA–LC4	RMA–WASP (2ot0)	RMA–NASEP (2ot1)
Beamline	22-BM (APS, ANL)	22-BM (APS, ANL)	X8-C (NSLS, BNL)
Space group	$P2_12_12_1$	$P2_1$	$P2_1$
Unit-cell parameters			
a (Å)	87.03	84.08	84.78
b (Å)	118.18	56.71	103.44
c (Å)	175.90	156.19	83.60
β (°)		97.78	98.66
Resolution (Å)	44–2.2 (2.28–2.2)	50–2.2 (2.3–2.2)	50–2.2 (2.28–2.2)
Unique reflections	91491	74498	72049
$\langle I/\sigma(I)\rangle$	4.5 (1.8)	20.4 (5.8)	39.1 (12.9)
Completeness	98.7 (89.8)	99.9 (99.9)	99.4 (98.4)
Redundancy	6.9 (4.4)	3.6 (3.3)	3.7 (3.5)
$R_{\rm merge}(I)$†	0.143 (0.526)	0.049 (0.233)	0.039 (0.122)
$R_{\rm r.i.m.}$‡	0.180 (0.535)	0.103 (0.297)	0.069 (0.177)
$R_{\rm p.i.m.}$§	0.065 (0.194)	0.053 (0.156)	0.036 (0.093)
Mosaicity¶ (°)	0.098 [0.5]	0.546 [0.4]	0.858 [0.5]

† $R_{\rm merge} = \sum_{hkl}\sum_i |I_i(hkl) - \langle I(hkl)\rangle| / \sum_{hkl}\sum_i I_i(hkl)$. ‡ $R_{\rm r.i.m.} = \sum_{hkl}[N/(N-1)]^{1/2} \times \sum_i |I_i(hkl) - \langle I(hkl)\rangle| / \sum_{hkl}\sum_i I_i(hkl)$. § $R_{\rm p.i.m.} = \sum_{hkl}[1/(N-1)]^{1/2}\sum_i |I_i(hkl) - \langle I(hkl)\rangle| / \sum_{hkl}\sum_i I_i(hkl)$. ¶ Values in square brackets are the oscillation angle per frame.

3. Results

3.1. Crystal packing

We compared our new RMA–LC4 structure with two differently liganded RMA structures, RMA–NASEP and RMA–WASP, following least-squares superpositions using the *LSQKAB* program (Kabsch, 1976) from the *CCP*4 suite (Collaborative Computational Project, Number 4, 1994). The homotetramer of the RMA–LC4 structure superimposed with an overall root-mean-square deviation of 0.64 Å for RMA–NASEP (2ot1) and 0.8 Å for RMA–WASP (2ot0) for 1360 C^{α} atoms. Inspection of the superimposed structures revealed no positional deviation in the main chain and in the majority of side chains, even though there were changes in space group and unit-cell parameters following the changes in crystal packing between the structures.

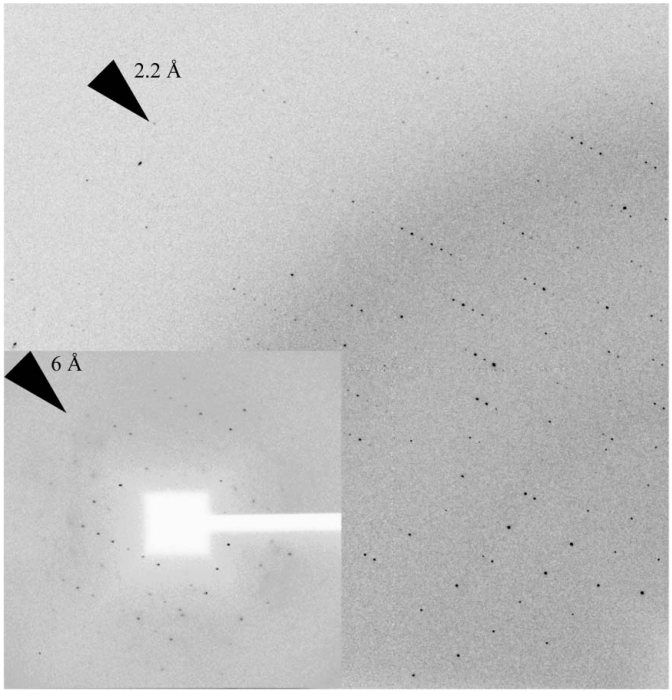

Figure 2
X-ray diffraction images from RMA–LC4 crystals grown both at room temperature (inset) and 277 K. The resolution limits are indicated.

Table 2
Crystallographic refinement statistics for three aldolase complex structures.

Values in parentheses are for the highest resolution shell.

	RMA–LC4	RMA–WASP (2ot0)	RMA–NASEP (2ot1)
Resolution (Å)	31–2.2 (2.28–2.2)	30–2.2 (2.3–2.2)	30–2.2 (2.26–2.2)
No. of reflections	91491	74498	72049
$R_{\rm cryst}$†	0.158 (0.233)	0.151 (0.249)	0.138 (0.156)
$R_{\rm free}$‡	0.194 (0.265)	0.191 (0.295)	0.180 (0.225)
R.m.s.d.			
Bond lengths (Å)	0.008	0.01	0.01
Bond angles (°)	1.03	1.03	1.04
Average B factors (Å^2)			
RMA	21.99	25.49	24.00
Ligand	34.68	59.90	55.62
No. of atoms			
Protein	10722	10744	10764
Water	1809	1801	1863
Ligand	455	157	101

† $R_{\rm cryst} = \sum_{hkl}\big||F_{\rm obs}| - |F_{\rm calc}|\big| / \sum_{hkl}|F_{\rm obs}|$. ‡ $R_{\rm free}$ was calculated with the removal of 5% of the data as the test set at the beginning of refinement.

Next, we compared the lattice constructions in the crystals by surveying the intermolecular interfaces. PDB entry 2ot0 interacts with six different neighboring tetramers with an interface area of 4290 Å^2, with the most extensive interaction interface consisting of 2919 Å^2 or up to 68% of the total interface area. The majority of the residues involved in this interaction, however, came from loop regions with an average temperature factor that was much higher than the noncontacting regions (Fig. 3). This same interaction interface was used for lattice formation in both crystal forms (*A* and *B*). However, their interaction was less extensive than that observed in the crystal with PDB entry 2ot0, with only 350 Å^2 (30% of the total interface) and 1618 Å^2 (52% of the total interface) of the surface area for crystal forms *A* and *B*, respectively.

3.2. Electron-density maps

We compared the quality of the data sets by visually inspecting the electron-density maps of the side chains of residues located in the tetramer interfaces and in the center of the molecules, where the structures are not affected by lattice-contact formation. The area of crystallographic contact and the ligand-binding region were excluded from the comparison. A total of 614 residues from each tetramer were compared. The electron-density maps of six residues of RMA–LC4 were better than those of 2ot0 and the electron density of eight residues were of better quality than those of 2ot1. On the other hand, 13 residues of the 2ot0 electron-density map and eight residues of the 2ot1 electron-density map were of better quality than those of RMA–LC4 (Fig. 4). Thus, the quality of the electron-density maps for these structures is comparable. The compared region had an average root-mean-square deviation of less than 0.29 Å.

The crystal lattice-packing interactions of RMA–LC4 are constructed through many high-entropy side chains. The side-chain electron density of these residues, which are involved in packing interactions, was well resolved, with the exception of Lys321 in subunit *C*. However, the same residues in 2ot0 and 2ot1 are largely disordered and often did not show interpretable electron density.

4. Discussion

We crystallized RMA in complex with the low-complexity domain (LC4) of sorting nexin 9 at room temperature, but the X-ray diffraction was poor as indicated by the large mosaic spread and

modest resolution. We were able to improve the quality of our RMA–LC4 crystals by lowering the crystallization temperature to 277 K and reducing the concentration of both protein and precipitant. Although the RMA–LC4 crystals grew larger at room temperature, their diffraction was limited to about 5 Å Bragg spacing. We also attempted to improve these crystals using the Proteros Free Mounting system with various humidity gradients, with no improvement in the observed X-ray diffraction quality (Kiefersauer *et al.*, 2000).

Our data set from RMA–LC4 crystals grown at 277 K stands out, with a low mosaic spread (0.1°) compared with all of the liganded RMA crystals that we have collected over the past decades, which had mosaic spreads of 0.5° or greater. Reduced mosaicity in crystals is manifested by an enhanced signal-to-noise ratio of the reflection intensities and is therefore particularly valuable for measuring the weak signal in high-resolution diffraction data (Bellamy *et al.*, 2000). Even though higher diffraction X-ray data could be obtained for 2ot0 and 2ot1, the quality of the electron-density map of RMA–LC4 was comparable to that of 2ot0 and 2ot1 and in certain areas the electron-density map was much clearer.

Both crystal forms *A* and *B* as well as PDB entry 2ot0 make crystallographic contacts with at least six independent neighboring tetramers and have a total buried interface area ranging from 1173 Å^2 (for form *A*) to 4290 Å^2 (for 2ot0). Intuitively, the total surface area involved in crystallographic packing would inversely correlate with mosaicity owing to the stability caused by the interaction surfaces. However, comparison of RMA–LC4 with other RMA crystals shows that the aforementioned notion does not correlate with the reduced mosaicity of RMA–LC4 crystals. Rather, the quality of the contact appears to be more important than the quantity of contacts. Indeed, RMA–LC4 crystals grown at 277 K use the largest number of high-entropy side chains in establishing lattice-packing contacts: of the 18 directional interactions, seven involve Gln residues, six involve Glu residues and another six use Lys residues (Juers & Matthews, 2001). In comparison, PDB entry 2ot0, which has the next highest number of interactions (17), has only two interactions involving Gln residues and four involving Glu residues, while only four involve Lys residues. The remaining crystal forms use substantially lower numbers of residues with high-entropy side chains in establishing packing interactions. In all crystal forms, the carboxy-terminal Tyr interacts identically with high-entropy side chains (Lys12, Gln202 and Arg258). In PDB entry 1ado and RMA–LC4 this same interaction bridges to an adjacent tetramer in the lattice.

The difference in the pH of the crystallization conditions of 7.1 at room temperature *versus* 7.6 at 277 K is a consequence of the temperature-dependence of the pH of the Tris buffer used in the

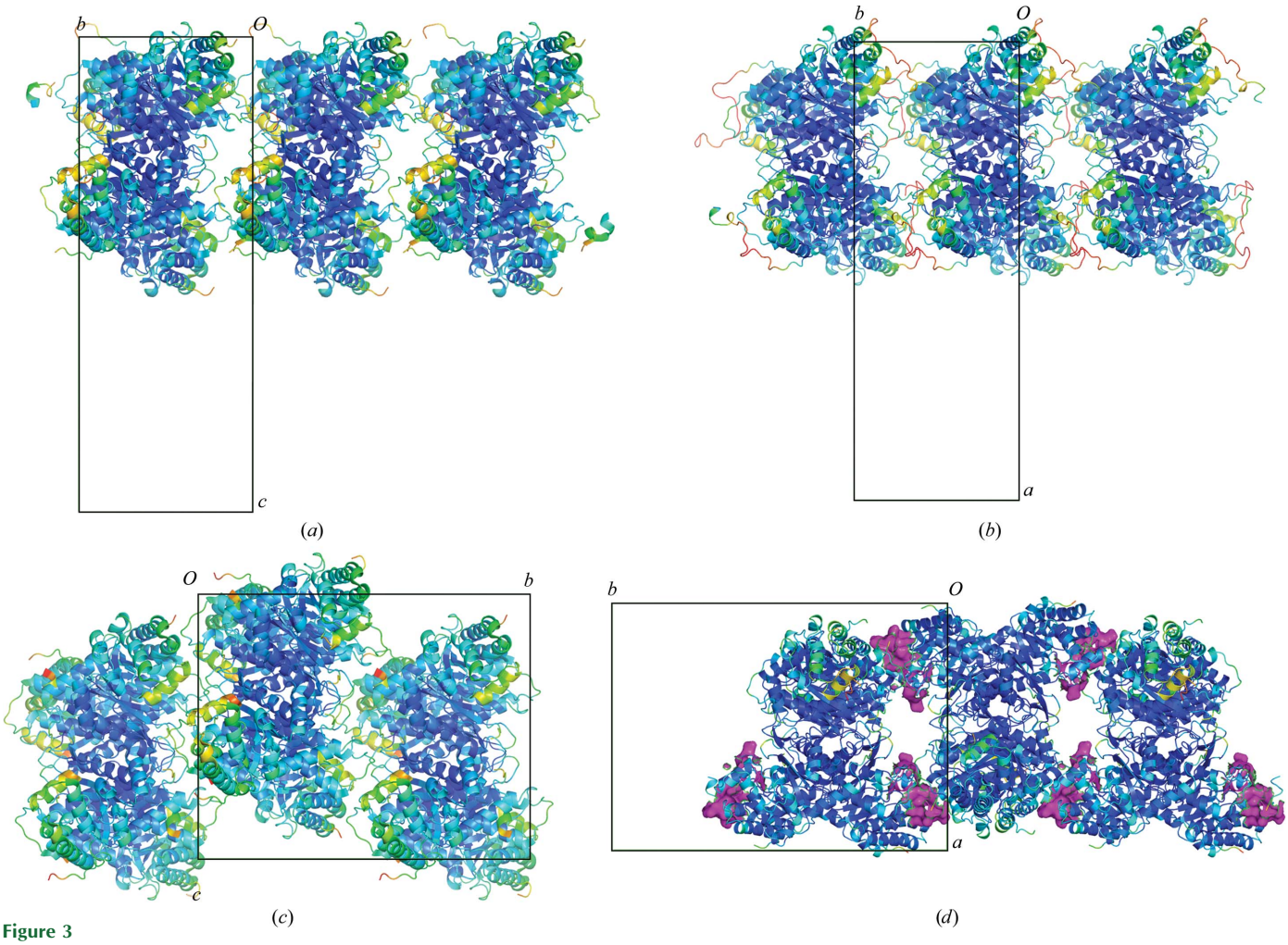

Figure 3
Illustration of the molecular packing projected along (*a*) the *a* axis for 2ot0, (*b*) the *c* axis for 1ado, (*c*) the *a* axis for 2ot1 and (*d*) the *c* axis for RMA–LC4. Except for RMA–LC4, the contact interfaces between molecules are dominated by loop regions with high temperature factors. The LC4 peptides bound to RMA that are involved in crystallographic contacts are rendered in magenta. A rainbow color scheme is used to show the relative temperature factors (blue, low temperature factor; red, high temperature factor). This figure was generated using *PyMOL* (DeLano, 2002).

crystallization solution (Bates & Hetzer, 1961). Although nucleation and crystal-growth processes are pH-dependent, the temperature-induced change of 0.5 pH units in the experimental conditions does not change the energetics of the crystal-packing interactions, since all of the interacting side chains have solution ionization potentials that differ by at least three pH units from that of the experimental conditions. This large difference in pK_a with respect to the pH of the crystallization solutions precludes redistribution of the populations of ionizable species of the interacting side chain owing to the temperature-induced pH change, and thus does not perturb the strength of the side-chain interactions used in lattice packing. For instance, in case of a lysine residue ($pK_a = 10.5$) an increase of 0.5 pH units would merely shift the ratio of neutral to ionized species from 0.04% to 0.16% and would negligibly decrease (by <0.04 kJ mol^{-1}) the energetic gain of 12.6 kJ mol^{-1} for a lysine participating in an electrostatic interaction (Fersht *et al.*, 1985). Similarly, hydrogen-bonding interactions, although twofold to fivefold weaker than electrostatic interactions (Fersht *et al.*, 1985), would also not be perturbed by the temperature-induced pH change in the experimental conditions. As a result, lattice interactions for all crystal forms are essentially insensitive to pH under the experimental conditions described. Although the temperature-induced pH shift can influence protein solubility and surface charge, because lattice formation is insensitive to pH over the experimental conditions, the temperature-induced pH changes of these parameters would serve to modulate the kinetics of protein crystal growth, namely the rates of nucleation and crystal growth, and not the lattice packing.

The thermodynamic cost of immobilizing high-entropy side chains tends to inhibit their participation in crystal-packing contacts and impedes successful crystal structure determination (Price *et al.*, 2009). Interactions implicating high-entropy side chains can occur upon cryocooling a protein crystal from room temperature, as the side chains of these residues become thermodynamically easier to order (Juers & Matthews, 2001). This side-chain ordering accompanying cryocooling is associated with an increase in crystal mosaicity, which is attributed to a change in unit-cell packing that induces strain. Although such an interpretation cannot be excluded in the case of RMA–LC4, the very low mosaicity value observed for the cryocooled crystals would argue against such a possibility and suggest that these side chains were ordered prior to cryocooling.

Surface side-chain ordering in the RMA–LC4 crystals grown at 277 K increases the interaction energy among the aldolase tetramers, thus strengthening lattice packing, which in turn minimizes the lattice strain incurred upon cryocooling and thereby reduces or inhibits changes in mosaicity. It is noteworthy that the solvent content of RMA–LC4 is 53.8%, compared with 50.6, 46.8 and 45.4% for PBD entries 1ado, 2ot1 and 2ot0, respectively, and would allow us to argue that in these RMA–LC4 crystals, the entropic loss owing to side-chain ordering could be offset by an entropy increase resulting from the larger bulk-solvent content of the unit cell. Intriguingly, the crystallization of RMA–LC4 at room temperature requires a nearly twofold increase in precipitant compared with RMA–LC4 crystallized at 277 K (25% PEG MME 550 *versus* 14% PEG MME 550, respectively). At room temperature, hydration data for PEG–water mixtures indicate that each PEG 600 molecule is hydrated by 31.2 water molecules, compared with 34.2 molecules at 277 K (Branca *et al.*, 2002), indicating that a significantly smaller total number of water molecules are involved in hydrating PEG in crystallization conditions at 277 K compared with room temperature. Although PEG MME differs from PEG by the presence of a methyl end group instead of a hydroxyl group, it would not significantly affect these conclusions as it merely reduces the number of water molecules that hydrate PEG MME by two. The significantly increased hydration by water molecules by nearly a factor of two at room temperature reduces the bulk-

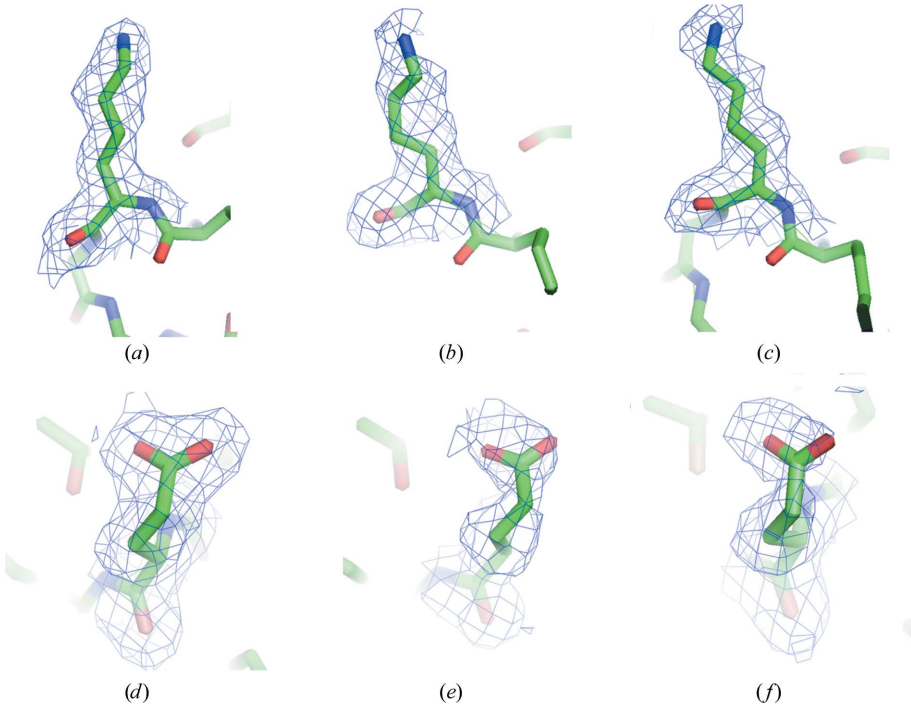

Figure 4
Area of the $2F_o - F_c$ electron-density map showing (*a*–*c*) Lys*A*139 and (*d*–*f*) Glu*B*10 contoured at 1σ. (*a*) and (*d*) RMA–LC4; (*b*) and (*e*) 2ot0; (*c*) and (*f*) 2ot1. All three structures were refined to 2.2 Å resolution. Although 2ot0 and 2ot1 showed better merging statistics, the RMA–LC4 electron-density map was clearer in certain areas, including the area exemplified here. The average real-space correlation coefficients for side-chain atoms calculated with *PHENIX* v.1.5 (Adams *et al.*, 2002) were (*a*) 0.944, (*b*) 0.78, (*c*) 0.771, (*d*) 0.947, (*e*) 0.931 and (*f*) 0.908.

solvent entropy, which would promote side-chain disorder at room temperature as a means of offsetting entropy reduction. This entropy compensation mechanism that increases the likelihood of disordered lattice-packing interactions at room temperature would consequently be incompatible with low mosaicity measurements using cryocooled crystals. Strengthened packing interactions as described would serve to enhance lattice long-range order and mitigate against degradation of resolution limits upon cryocooling.

We are grateful to the staff at the Advanced Photon Source, SER-CAT for synchrotron support. TI is supported by grants from the National Institutes of Health and by start-up funds provided to Scripps Florida from the State of Florida. This is publication No. 20117 from the Scripps Research Institute. JS was supported by funding from the Natural Science and Engineering Research Council (Canada).

References

Adams, P. D., Grosse-Kunstleve, R. W., Hung, L.-W., Ioerger, T. R., McCoy, A. J., Moriarty, N. W., Read, R. J., Sacchettini, J. C., Sauter, N. K. & Terwilliger, T. C. (2002). *Acta Cryst.* D**58**, 1948–1954.
Bates, R. G. & Hetzer, H. B. (1961). *J. Phys. Chem.* **65**, 667–671.
Bellamy, H. D., Snell, E. H., Lovelace, J., Pokross, M. & Borgstahl, G. E. O. (2000). *Acta Cryst.* D**56**, 986–995.
Bergfors, T. (1999). *Protein Crystallization: Techniques, Strategies and Tips: A Laboratory Manual.* La Jolla: International University Line.
Blanc, E., Roversi, P., Vonrhein, C., Flensburg, C., Lea, S. M. & Bricogne, G. (2004). *Acta Cryst.* D**60**, 2210–2221.
Blom, N. & Sygusch, J. (1997). *Nature Struct. Biol.* **4**, 36–39.
Branca, C., Magazu, S., Maisano, G., Migliardo, F., Migliard, P. & Romeo, G. (2002). *J. Phys. Chem. B*, **106**, 10272–10276.
Collaborative Computational Project, Number 4 (1994). *Acta Cryst.* D**50**, 760–763.
DeLano, W. L. (2002). *PyMOL Molecular Viewer.* http://www.pymol.org.
Derewenda, Z. S. & Vekilov, P. G. (2006). *Acta Cryst.* D**62**, 116–124.
Eagles, P. A., Johnson, L. N., Joynson, M. A., McMurray, C. H. & Gutfreund, H. (1969). *J. Mol. Biol.* **45**, 533–544.
Ellis, J., Campopiano, D. J. & Izard, T. (1999). *Acta Cryst.* D**55**, 1086–1088.
Emsley, P. & Cowtan, K. (2004). *Acta Cryst.* D**60**, 2126–2132.
Fersht, A. R., Shi, J. P., Knill-Jones, J., Lowe, D. M., Wilkinson, A. J., Blow, D. M., Brick, P., Carter, P., Waye, M. M. & Winter, G. (1985). *Nature (London)*, **314**, 235–238.
Hurlbert, J. & Izard, T. (2002). *Acta Cryst.* D**58**, 1749–1751.
Izard, T., Sarfaty, S., Westphal, A., de Kok, A. & Hol, W. G. (1997). *Protein Sci.* **6**, 913–915.
Juers, D. H. & Matthews, B. W. (2001). *J. Mol. Biol.* **311**, 851–862.
Kabsch, W. (1976). *Acta Cryst.* A**32**, 922–923.
Kiefersauer, R., Than, M. E., Dobbek, H., Gremer, L., Melero, M., Strobl, S., Dias, J. M., Soulimane, T. & Huber, R. (2000). *J. Appl. Cryst.* **33**, 1223–1230.
Krissinel, E. & Henrick, K. (2007). *J. Mol. Biol.* **372**, 774–797.
Ng, J. D., Lorber, B., Giegé, R., Koszelak, S., Day, J., Greenwood, A. & McPherson, A. (1997). *Acta Cryst.* D**53**, 724–733.
Otwinowski, Z. & Minor, W. (1997). *Methods Enzymol.* **276**, 307–326.
Price, W. N. II *et al.* (2009). *Nature Biotechnol.* **27**, 51–57.
Rangarajan, E. S., Park, H., Fortin, E., Sygusch, J. & Izard T. (2010). *J. Biol. Chem.* **285**, 11983–11990.
St-Jean, M., Izard, T. & Sygusch, J. (2007). *J. Biol. Chem.* **282**, 14309–14315.
Sygusch, J., Beaudry, D. & Allaire, M. (1987). *Proc. Natl Acad. Sci. USA*, **84**, 7846–7850.
Vagin, A. & Teplyakov, A. (1997). *J. Appl. Cryst.* **30**, 1022–1025.
Yeh, J. I. & Hol, W. G. J. (1998). *Acta Cryst.* D**54**, 479–480.